

This document is confidential and is proprietary to the American Chemical Society and its authors. Do not copy or disclose without written permission. If you have received this item in error, notify the sender and delete all copies.

Studies of dynamic binding of amino acids to TiO₂ nanoparticle surfaces by Solution NMR and Molecular Dynamics Simulations

Journal:	<i>Langmuir</i>
Manuscript ID	la-2020-012568.R2
Manuscript Type:	Article
Date Submitted by the Author:	20-Jul-2020
Complete List of Authors:	xue, mengjun; University of Washington, Department of Chemistry Sampath, Janani; University of Washington , Gebhart, Rachel; University of Washington Seattle Campus, Chemistry Haugen, Havard; Universitetet i Oslo, Institute for Clinical Dentistry, Department Biomaterials Lyngstadaas, Stale ; University of Oslo, Department for Biomaterials, Faculty for Odontology Pfaendtner, Jim; University of Washington, Chemical Engineering Drobny, Gary; University of Washington, Chemistry

SCHOLARONE™
Manuscripts

Studies of dynamic binding of amino acids to TiO₂ nanoparticle surfaces by Solution NMR and Molecular Dynamics Simulations

Mengjun Xue,¹ Janani Sampath,² Rachel N. Gebhart,¹ Havard J. Haugen,³

S. Petter Lyngstadaas,³ Jim Pfaendtner,² Gary Drobny^{1,}*

1. Department of Chemistry, University of Washington Box 351700, Seattle, Washington 98195, United State
2. Department of Chemical Engineering, University of Washington Box 351700, Seattle, Washington 98195, United States
3. Department for Biomaterials, Faculty for Odontology, University of Oslo, PO Box 1109 Blindern, NO-0317 Oslo, Norway

ABSTRACT

Adsorption of biomolecules onto material surfaces involves a potentially complex mechanism where molecular species interact to varying degrees with a heterogeneous material surface. Surface adsorption studies by atomic force microscopy (AFM), Sum Frequency Generation (SFG) spectroscopy, and solid state NMR (ssNMR), detect the

1
2
3 structures and interactions of biomolecular species that are bound to material surfaces
4
5
6
7 and which, in the absence of a solid liquid interface, do not exchange rapidly between
8
9
10 surface-bound forms and free molecular species in bulk solution. Solution NMR has the
11
12
13 potential to complement these techniques by detecting and studying transiently bound
14
15
16
17 biomolecules at the liquid-solid interface. Herein we show that dark-state exchange
18
19
20 saturation transfer (DEST) NMR experiments on gel-stabilized TiO_2 nanoparticle (NP)
21
22
23 samples detect several forms of biomolecular adsorption onto titanium (IV) oxide
24
25
26
27 surfaces. Specifically, we use the DEST approach to study the interaction of amino acids
28
29
30 arginine (Arg), lysine (Lys), leucine (Leu), alanine (Ala), and aspartic acid (Asp) with TiO_2
31
32
33
34 rutile nanoparticle surfaces. Whereas Leu, Ala, and Asp display only a single weakly
35
36
37
38 interacting form in the presence of TiO_2 nanoparticles, Arg and Lys displayed at least two
39
40
41
42 distinct bound forms: a species that is surface bound and retains a degree of
43
44
45 reorientational motion, and a second more tightly bound form characterized by broadened
46
47
48 DEST profiles upon addition of TiO_2 nanoparticles. Molecular Dynamics simulations
49
50
51
52 indicate different surface bound states for both Lys and Arg depending on the degree of
53
54
55
56 TiO_2 surface hydroxylation, but only a single bound state for Asp regardless of the degree
57
58
59
60

1
2
3 of surface hydroxylation, in agreement with results obtained from analysis of DEST
4
5
6
7 profiles.
8
9

11 INTRODUCTION

12
13
14 The interaction of biomolecules with titanium (IV) oxide (TiO_2) nanoparticles (NP's) is a
15 topic relevant to a variety of fields including medical and dental implants, biosensors,
16 chromatography, and catalysis.¹⁻¹² Fundamental to our understanding of how biomolecules interact
17 with TiO_2 NP's is knowledge of the structures of these molecules at NP surfaces. However,
18 detailed structural information of surface-adsorbed peptides is only now emerging,¹³⁻¹⁵ and the
19 nature of protein-mineral surface interactions has yet to be clarified even for small monomeric
20 amino acids and small mineral-binding peptides. Methods used to detect and characterize surface-
21 bound molecular species include Atomic Force Microscopy (AFM),¹⁶⁻¹⁸ Sum Frequency
22 Generation (SFG) Spectroscopy,¹⁹⁻²⁰ Solid State NMR (ssNMR),²¹ Saturation Transfer Difference
23 NMR²² to name a few. These methods detect the presence of partly or entirely immobilized
24 biomolecular species at material surfaces where the amino acid side chains provide points of
25 surface contact.
26
27
28
29
30
31
32
33
34
35
36
37
38
39
40
41

42 The mechanism of surface adsorption of biomolecules onto TiO_2 NP's is complex and may
43 involve, prior to final attachment and immobilization on the surface, formation of biomolecular
44 species that interact with and are only partly immobilized near the NP surface. In addition, the
45 material surface may be heterogeneous, resulting in a variation in binding affinity over the surface
46 and in multiple forms of bound species. Because they are the monomeric constituents of proteins,
47 adsorption of amino acids onto metallic and oxide surfaces has been widely studied. Although
48
49
50
51
52
53
54
55
56
57
58
59
60

1
2
3 thermodynamic studies of lysine^{23,24} and histidine²⁵ adsorption onto TiO₂ NP's fitted data using a
4 simple Langmuir model, which assumes a single affinity constant and a single independently
5 bound form, spectroscopic studies have identified more complex scenarios for adsorption of some
6 amino acids on TiO₂ NP's. A IR spectroscopic study of the binding of glutamic acid and aspartic
7 acid to TiO₂ NP's found that while at all pH's aspartic acid binds in a single form, glutamic acid
8 binds in at least two forms.²⁶ A very recent thermodynamic study of the adsorption of L-amino
9 acids onto TiO₂ NP's found that the BET model fits the binding of most amino acids to TiO₂, with
10 the binding being endothermic and thus entropy driven.²⁷ In the same study computations showed
11 surface interactions via hydrogen bonding between the α -ammonium group and surface hydroxyl
12 oxygens, while basic and acid amino acids can also interact with the surface via their side chains.
13
14
15
16
17
18
19
20
21
22
23
24
25

26 In view of the complex nature of amino acid and peptide adsorption onto TiO₂ NP's, it is
27 useful to apply experimental techniques that can detect several types of adsorbed species, under
28 the same sample conditions. Dark-state exchange saturation transfer (DEST) NMR
29 experiments have provided thermodynamic and kinetic information on the binding of small
30 proteins to aggregates and large molecular machines.²⁸⁻³⁰ DEST relies on slow exchange
31 of nuclear spins between sites with very different values of the transverse relaxation rate
32 R_2 , as would occur for example when a freely tumbling molecular species in solution with
33 a small R_2 , adsorbs onto a TiO₂ NP surface with the resulting immobilized species
34 displaying a much larger R_2 . In addition to R_2 values for free and bound molecular species,
35 simulation of the DEST saturation profile yields further information, including the relative
36
37
38
39
40
41
42
43
44
45
46
47
48
49
50
51
52
53
54
55
56
57
58
59
60

1
2
3 populations of the free and adsorbed species, and the kinetic constants that quantify the
4
5
6
7 rate of exchange between free and adsorbed species. In an initial demonstration of this
8
9
10 approach, Egner et al.³¹ applied ¹H DEST and relaxation dispersion (RD) to the study of
11
12
13 the adsorption of phenol and cholic acid onto cerium oxide NP's. By direct solution of the Bloch-
14
15 McConnell equations and subsequent simulation of the ¹H DEST saturation profiles, Egner et al
16
17 showed that while cholic acid adsorbs from bulk solution to a weakly-bound state that does not
18
19 constitute a rigid adduct with the NP, phenol adsorption proceeds via an intermediate, weakly
20
21 bound species to a state that is rigidly bound to the NP surface. Therefore, the Egner et al. study
22
23 afforded not only populations of free and bound species, but also a kinetic mechanism for the
24
25 adsorption process.
26
27
28
29

30 MD simulations have also provided valuable insights into the binding mechanism
31
32
33 of amino acids and their analogs on the surface of TiO₂.³²⁻³⁶ Bowen et al. found that the
34
35
36 adsorption of amino acids with polar sidechains on a negative rutile (110) surface is a
37
38
39 function of both backbone and sidechain binding.³² Walsh and coworkers studied the
40
41
42 binding of arginine, aspartate and lysine analogs on two variants of the rutile interface –
43
44
45 negative and neutral; they report that the arginine analog adsorbed the strongest to both
46
47
48
49
50 interfaces, followed by the lysine and aspartate analogs.^{35,36} Recently, Schelokov et al.
51
52
53
54 described the adsorption of amino acids on nanocrystalline anatase particles using QSPR
55
56
57
58
59
60

1
2
3 and MD simulations, they find that the binding occurs primarily through the formation of
4
5
6
7 two – three hydrogen bonds via sidechain or backbone groups that are charged.²⁷
8
9

10 In this paper we apply ¹H DEST techniques to the study of the adsorption of small
11
12
13 biomolecules, i.e. amino acids, to TiO₂ rutile nanocrystals. Application of DEST methods
14
15
16
17 to studying the binding of biomolecules to mineral surfaces has the same requirements
18
19
20
21 detailed in the study of Egner et al.³¹ Namely, the NMR-visible molecules (i.e. the free,
22
23
24 unbound molecules) and the NMR-invisible molecules (i.e. the surface-bound molecules)
25
26
27
28 have to remain homogeneously suspended in the NMR sample throughout the NMR
29
30
31 measurement period. We followed the procedure described in Egner et al. and used 1
32
33
34 wt% agarose to prevent nanoparticle sedimentation. By introducing TiO₂ nanocrystals into
35
36
37
38 agarose gel suspensions, we investigated the binding of arginine (Arg), lysine (Lys),
39
40
41
42 leucine (Leu), aspartate (Asp), and alanine (Ala) amino acid. We chose amino acids as
43
44
45
46 model systems for initial study because they contain the same side chain functional
47
48
49 groups used by peptides and proteins to adsorb onto TiO₂ NP surfaces,¹⁶⁻¹⁸ yet their small
50
51
52
53 size limits the number of surface-bound forms that may be present. Lorentzian
54
55
56
57 deconvolution of ¹H DEST saturation profiles indicate for Arg and Lys the existence of
58
59
60

1
2
3 multiple forms of adsorbed molecules, distinguished by differing degrees of residual
4
5
6
7 molecular motion. Simulation of the ^1H DEST profiles by direct solution of the Bloch-
8
9
10 McConnell equation provides quantitative information including relative populations of
11
12
13 free and adsorbed species as well as kinetic constants that quantify rate of exchange
14
15
16
17 between free and adsorbed species. Finally, molecular dynamics simulations also
18
19
20 demonstrate the existence of multiple binding states of Arg and Lys on rutile surfaces,
21
22
23 and investigate the role played by surface hydroxylation in mediating these interactions.
24
25
26
27 Overall this paper demonstrates how the application DEST NMR experiments and MD
28
29
30 calculations in a concerted fashion can elucidate both thermodynamic and kinetic aspects
31
32
33 of the adsorption of biomolecules at liquid-solid interfaces.
34
35
36
37
38

39 EXPERIMENTAL

40
41 **Materials.** Amino acids alanine, leucine, arginine, lysine, and aspartic acid were purchased from
42
43 Sigma-Aldrich (St. Louis, MO) and used without purification. TiO_2 (product number 637262;
44
45 rutile titanium (IV) oxide nanopowder with a reported particle size <100 nm) nanoparticles were
46
47 purchased from Sigma-Aldrich (St. Louis, MO) with a BET measured surface area of $28.6 \text{ m}^2/\text{g}$.
48
49 Agarose were purchased from Sigma Aldrich and used without further purification. Deuterated
50
51 solvents were purchased from Sigma Aldrich and used without further purification.
52
53
54
55
56
57
58
59
60

1
2
3 **Preparation of NMR samples.** 10 mM Amino acids (Arg, Lys, Leu, Pro, Asp, and Ala) NMR
4 samples were prepared in 20 mM phosphate buffer pD7 with 99.9% D₂O.
5
6

7
8
9 Samples without TiO₂ nanopowder in the presence of agarose gel were prepared by mixing 1%
10 w/w agarose in 20 mM phosphate buffer (pD 7, 99.9% D₂O). The mixture was placed in a boiling
11 water bath for 5 min, then removed to a block heater to cool. When the temperature of equilibrated
12 water bath for 5 min, then removed to a block heater to cool. When the temperature of equilibrated
13 to between 50 and 60 °C, amino acid solution was added, resulting in a final concentration of 10
14 mM. The warm solution was transferred to an NMR tube and allowed to cool at room temperature.
15
16
17

18
19
20
21 Samples that contained TiO₂ nanopowder in the presence of gel were prepared by mixing 1% w/w
22 TiO₂ nanopowder and agarose in 20 mM phosphate buffer (pD 7, 99.9% D₂O). The mixture was
23 vortex mixed and sonicated for 5 min, then placed in a boiling water bath for 5min. The sample
24 was then removed to a block heater and its internal temperature allowed to equilibrate between 50-
25 60 °C. The respective amino acid solution was added, resulting in a final concentration of 10mM.
26
27
28
29
30
31
32
33 The warm solution was transferred to an NMR tube and allowed to cool to room temperature.
34
35

36 **NMR spectroscopy.** The NMR measurements were performed at 25 °C on a Bruker
37 Avance III 700 MHz NMR instrument equipped with a 5 mm Broadband Observe (BBO)
38 probe. ¹H-DEST experiments were measured at multiple saturation fields (50 Hz, 100 Hz, 150
39 Hz, 200 Hz, 250 Hz and 300 Hz) using a ¹H DEST pulse scheme.³¹ 1D ¹H spectra were recorded
40 in steps of 0.25 or 2.5 ppm with the position of the ¹H B1 field ranging from -100 ppm to +100
41 ppm, and an offset of -100 ppm was used for normalization. The saturation field was applied for 1
42 s, and a repetition delay of 3 s. NMR spectra were processed using Topspin 4.0.2 and Mnova NMR
43 (http://mestrelab.com/software/mnova/nmr/). Spectra were analyzed using Bruker dynamics
44
45
46
47
48
49
50
51
52
53
54
55
56
57
58
59
60

center (<https://www.bruker.com/products/mr/nmr/nmr-software/software/dynamics-center/overview.html>.) and Mnova NMR.

Analysis of data. Data were processed with Peak Analyzer in OriginPro (OriginLab Corporation, Northampton, MA, USA). Z-spectra (I/I_0) (or DEST profile) were normalized by the signal with RF irradiation at -100 ppm (I_0). For the conventional fitting method, multi-pool Lorentzian fitting of the Z-spectra was applied to estimate the DEST effects from different pools.³⁷⁻³⁹ Briefly, the inverted Z-spectra ($1-I/I_0$) were fitted as the sum of multiple Lorentzian functions with the following equation:

$$1 - \frac{I}{I_0} = \sum_{i=1}^N \frac{A_i}{1 + 4 \left(\frac{\omega - \omega_i}{\sigma_i} \right)^2} \quad (1)$$

where ω is the frequency offset from the interest resonance, A_i , ω_i , and σ_i are the amplitude, frequency offset and linewidth of the DEST peak for the i^{th} proton pool respectively. In the DEST phantom, we employed a four-pool or five-pool Lorentzian model of magnetization transfer (MT), and Nuclear Overhauser enhancement (NOE) effects from bound water and/or nearby hydrogens in molecules.⁴⁰⁻⁴¹

Global fitting was accomplished with a homogenous form of McConnell equations using Matlab code DESTfit (<https://spin.niddk.nih.gov/cloure/Software/software.html>).²⁸ A single spin was assumed to be in exchange between an observable free state with low R_2 and a two types of bound forms with larger R_2 values (A \rightleftharpoons the mixture of B and C).²⁸ The cross-relaxation between two spins was incorporated in the McConnell model: the cross-

1
2
3 relaxation rate σ_A between H_1 (the observed signal) and H_2 (coupled with H_1 by cross
4
5
6
7 relaxation) in the free amino acid is assumed to be -0.5 s^{-1} , and the cross-relaxation rate
8
9
10 σ_B between H_1 and H_2 of amino acid bound on particle is assumed to be -500 s^{-1} .²⁸

11
12
13 **Molecular Dynamics Calculations** The effects of molecular (non-hydroxylated TiO_2) and
14
15 dissociated (hydroxylated TiO_2) surface water were investigated for two variants of the rutile
16
17 (110), using the force field developed by Předota et al.⁴² The surface dimensions are approximately
18
19 $5.5 \times 5.3 \times 1.8 \text{ nm}^3$, and both surfaces are negatively charged with a charge density of -0.103 C/m^2 ,
20
21 corresponding to a pH of 8. Three amino acids were chosen for this study – aspartic acid (Asp),
22
23 lysine (Lys), and arginine (Arg); in the pD range of 7.5–8.0, the charges of the amino acid
24
25 sidechains are -1, +1 and +1, respectively. To remain comparable with the ^1H NMR experiment,
26
27 amino acid termini have a deprotonated carboxylate group and a protonated amine group. The
28
29 amino acids were modeled using the CHARMM36 forcefield.⁴³ A water slab 8nm thick consisting
30
31 of ~7500 molecules of SPC/E water was added above the surface. System equilibration was carried
32
33 out using a Donadio-Bussi-Parrinello⁴⁴ and a Parrinello-Rahman⁴⁵ barostat to maintain a
34
35 temperature and pressure of 300K and 1 bar, respectively. After equilibrating the system at 1bar
36
37 and 300K, well-tempered metadynamics⁴⁶ was employed to calculate binding free energy profiles
38
39 by biasing the vertical distance of the peptide from the surface (see Supporting Information for
40
41 details). Simulations were performed using GROMACS 5.1.2,⁴⁷ along with the PLUMED plugin⁴⁸
42
43 for enhanced sampling.
44
45
46
47
48
49
50
51

52 RESULTS AND DISCUSSION

53
54
55
56
57
58
59
60

¹H DEST NMR Studies of the interactions of amino acids Arg, Lys, Asp, Leu and Ala with TiO₂ NPs in Agarose Gels. The addition of TiO₂ (1 wt%) to a 10 mM amino acid solution in 99.9% D₂O resulted in extensive line broadening of the NMR resonances in all cases (Figure 1, and Figure S1), thus indicating that Arg, Lys, Asp, Leu and Ala all interact with TiO₂ and exchange between a free and a bound state. A lesser degree of peak broadening is observed upon the addition of agarose gel to the sample, indicating that the amino acids are weakly interacting with the matrix, but retain the ability to diffuse and tumble freely.

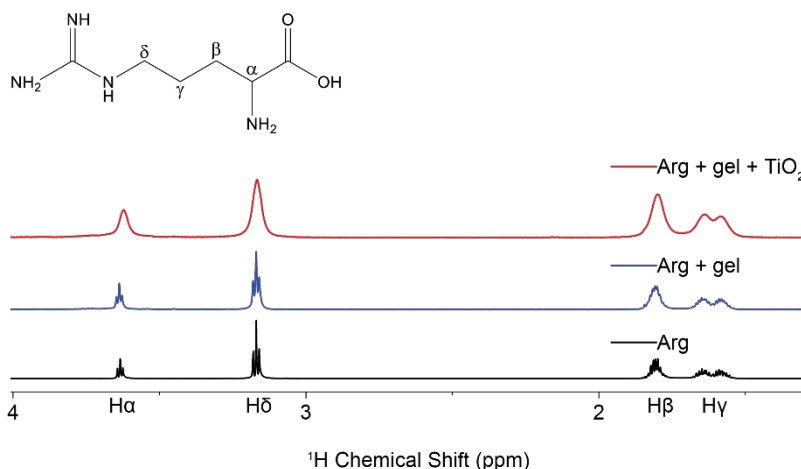
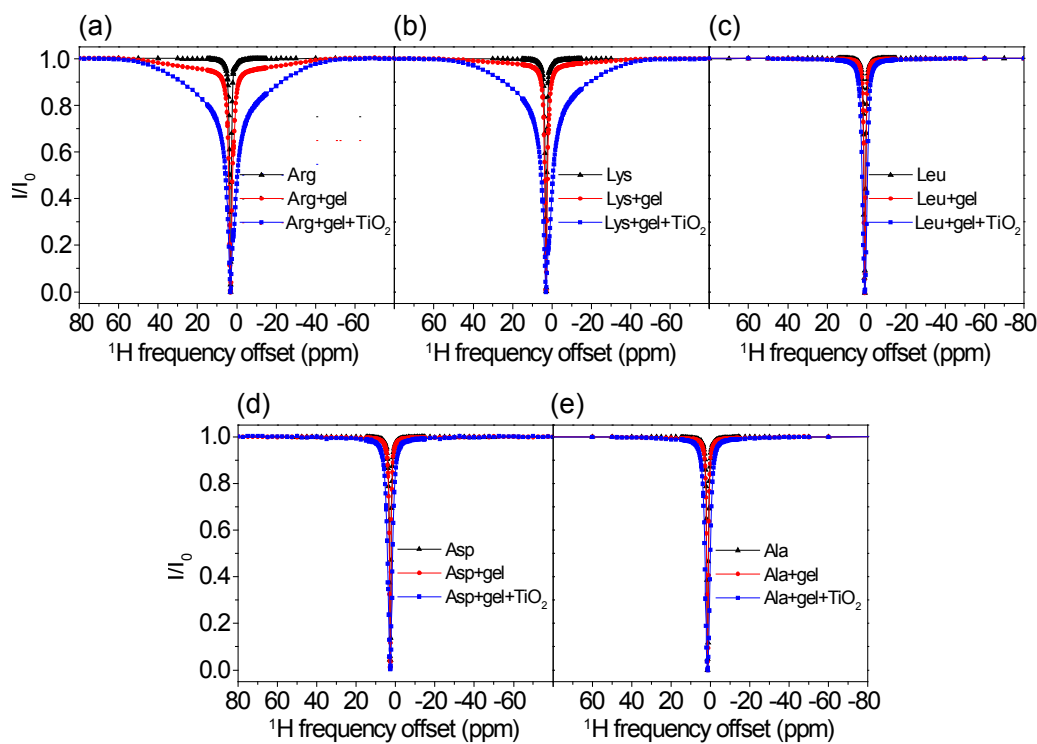


Figure 1. ¹H proton spectra of arginine neat (black), suspended in agarose gel (blue), and exposed to TiO₂ nanoparticles in the presence of agarose gel (red). Addition of TiO₂ to the sample creates distinct peak broadening not observed in the other two spectra, indicative of interactions with a slow tumbling object.

In DEST NMR experiments slow exchange and by inference contact with NP surfaces, is indicated by broadening of the DEST saturation profile upon addition of agarose gel and TiO₂ NPs. Figure 2 shows the ¹H DEST profiles of side chain protons for five monomeric amino acids (Arg, Lys, Leu, Asp, and Ala): 1) free in solution (10mM), 2) in the presence of agarose gel, and 3) in the presence of TiO₂ NPs and agarose gel. These amino acids

1
2
3
4 were chosen for their appearance in the hexamer peptide TBP-6, which has been shown
5
6
7 to bind strongly to rutile TiO_2 .¹⁶ Mutation studies of the peptide have suggested that the
8
9
10 three polar residues (Arg, Lys, and Asp) are involved in surface adhesion, while further
11
12
13
14 studies have suggested that non-polar residues may also play a role in surface
15
16
17 interactions.³²⁻³⁶ In the absence of TiO_2 NP's the DEST saturation profiles for H_ϵ of Lys
18
19
20 (Figure 2b) and H_δ of Arg (Figure 2a) are narrow and confined to <1 ppm region about the
21
22
23
24 respective resonance frequencies. In both cases there is a slight broadening of the
25
26
27
28 saturation profile upon addition of agarose gel (Figures 2a and 2b), indicating weak
29
30
31 interactions of these basic amino acids with the gel. Upon addition of TiO_2 NPs, the
32
33
34
35 saturation profiles of both Arg and Lys become broadened and display broad "wings"
36
37
38 indicative of slow exchange between the free state of the amino acid and a "dark", i.e.
39
40
41
42 surface-bound state, with a very large R_2 . The larger broadening of the Arg DEST profile
43
44
45 upon TiO_2 addition suggests that Arg has a greater affinity of binding to the nanoparticles
46
47
48
49 than Lys.
50
51
52
53
54
55
56
57
58
59
60

1
2
3
4 Figure 2c-e show analogous DEST saturation profiles for H β of Asp, H δ of Leu,
5
6
7 and H β of Ala respectively. In the three cases there is no broadening of the saturation
8
9
10 profile upon addition of agarose gel (Figure 2c-d), indicating no interactions of these
11
12
13 amino acids with the matrix. Interestingly, the Asp monomer as well as the nonpolar amino
14
15
16 acids do not show broad “wings” in their DEST profiles upon addition of TiO₂ NPs,
17
18
19 indicating that these individual amino acid monomers retain considerable re-orientational
20
21
22 degrees of freedom upon addition of TiO₂ NPs and as a result have much smaller R2
23
24
25 values than is the case with Arg and Lys.
26
27
28
29
30
31



32
33
34
35
36
37
38
39
40
41
42
43
44
45
46
47
48
49
50
51
52
53
54
55
56 **Figure**
57 **2.** ¹H DEST profiles for H δ of 10 mM Arg (a), H ϵ of 10 mM Lys (b), H δ of 10 mM Leu (c), H β of
58
59
60

1
2
3 Asp (d), and H β of 10 mM Ala (e) neat (black), with 1% w/w agarose gel (red), and with 1% w/w
4 agarose gel and 1% w/w TiO₂ nanoparticles (blue). Slight peak broadening of the DEST profile
5 upon addition of agarose gel for Arg and Lys (a-b) indicates a weak interaction between the agarose
6 gel and the amino acids, and broadening upon addition to TiO₂ indicates an interaction with the
7 oxide. In all figures B₁= 300 Hz.
8
9

10 In the case of Arg and Lys the ¹H DEST profiles in the presence of TiO₂ NPs are
11
12
13 asymmetric, indicating presence of spectral features in addition to the direct saturation
14
15
16 lines. Information on the origins of the broad asymmetric DEST profiles for Arg (Figure 3)
17
18 and Lys (Figure S2) may be obtained by a study of the DEST profiles as a function of ¹H
19
20
21 B₁ field strength. Figure 3 shows ¹H DEST profiles for the H δ proton of Arg: (a) free in 10
22
23
24 mM solution; (b) 10 mM concentration in agarose gel; and (c) 10mM concentration in
25
26
27
28 agarose gel and in the presence of TiO₂ NPs, for B₁ saturation fields ranging from 50-300
29
30
31 Hz. In all three figures a partial source of the asymmetry is traced in part to a line at a chemical
32
33
34 shift of 1.68 ppm. In Figure 3a this is the small feature out of phase with the direct saturation line,
35
36
37 while in Figure 3b and c the line at 1.68 ppm is in phase with the direct saturation line and is much
38
39
40 more intense. This 1.68 ppm line is therefore an NOE to neighboring H β and H γ protons. The fact
41
42
43 that the NOE inverts from positive to negative upon addition of gel indicates a slowing of
44
45
46 molecular reorientations, and the increase in the NOE intensity upon addition of TiO₂ NPs
47
48
49 indicates a further slowing of molecular reorientations due to strong interactions between the
50
51
52 amino acid and the TiO₂ NP surface.
53
54
55
56
57
58
59
60

From the line shapes in Figure 3c at least four components to the ^1H DEST saturation profile are discernable: 1) the direct $\text{H}\delta$ saturation component at 3.16 ppm, 2) the aforementioned NOE to neighboring side chain protons at 1.68 ppm, and 3) a component at about 4.73 ppm which is the NOE to the protons of surface-adsorbed water on TiO_2 particles; 4) a broad component most clearly observable in the 300 Hz. profile. In the DEST saturation profile of the $\text{H}\delta$ proton of Arg, this broad component is centered at about 3.16 ppm and corresponds to a surface immobilized molecular species. This broad component and strong NOE peak is also observed in the ^1H DEST profile for the $\text{H}\epsilon$ proton of Lys (Figure 2b, and Figure S2), but not in the DEST profiles for the side chain protons in Leu, Asp, or Ala (see Figures 2c-e, Figures S3-S5).

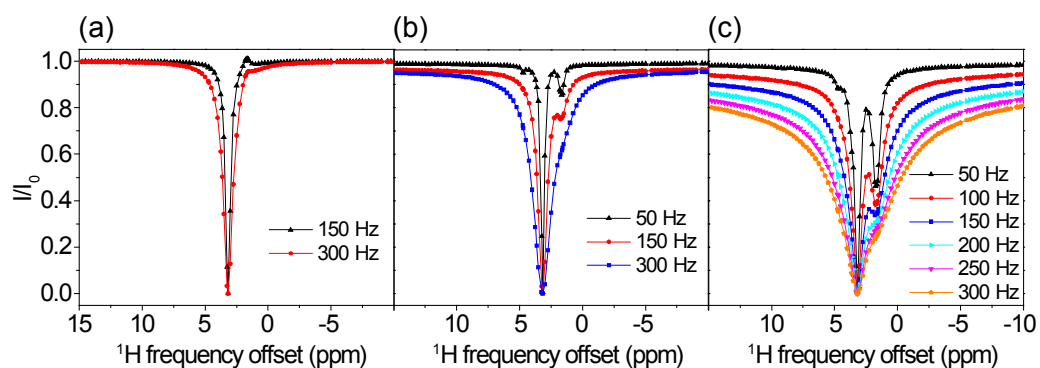
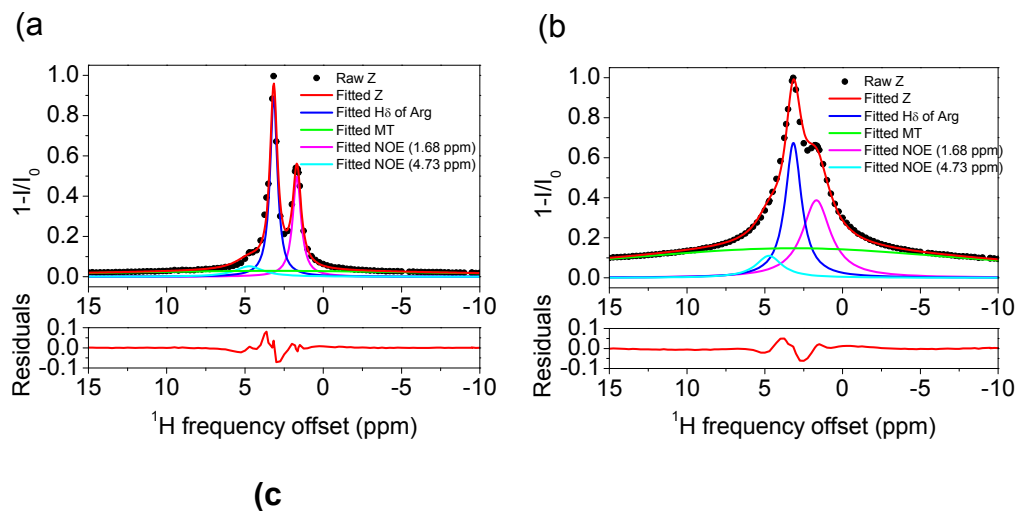


Figure 3. ^1H DEST profiles for $\text{H}\delta$ of 10 mM Arg in the absence of gel (a), in the presence of gel (b), and in the presence of gel and 1 wt % TiO_2 (c).

To confirm the assumption that ^1H DEST profiles for Arg in Figure 3 are interpreted in terms of four spectral components, inverted ^1H DEST saturation profiles of Arg (i.e. $1-I/I_0$) were fitted to Equation 1 for $B_1=50\text{-}300$ Hz. as described in the data analysis section (Figure 4a-c and Table S1-S3). It was assumed that the chemical shifts ω_i were constant for all B_1 values while A_i and σ_i were varied. As expected, the intensity of the NOE peaks and broad “wing” components

are enhanced with increasing B_1 saturation power, although the NOE peak intensities shows relatively less sensitivity to B_1 saturation power than the broad “wing” components (Table S1-S3). Several conclusions can be drawn from inspection of the fitted data. First, the good agreement between the fits and the data validate the four-component assumption. Second, the direct saturation line is in phase with the NOEs, i.e. the NOEs are negative. This indicates that Arg is tumbling slowly due to interactions with the NP surface. Third, the negative NOE to water is likely not due to magnetization transfer to bulk water but rather involves water that is bound to the TiO_2 NP surface. Finally, these simulations indicate presence of two bound forms of Arg: a weakly bound form which undergoes slow re-orientational motions and is closely associated with surface water molecules, and an immobilized form. A similar analysis has also been performed on the ^1H DEST profil for the H_ϵ proton of Lys with similar results (Figure S6).



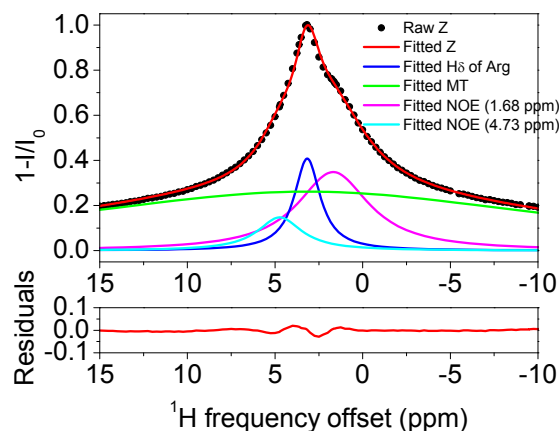
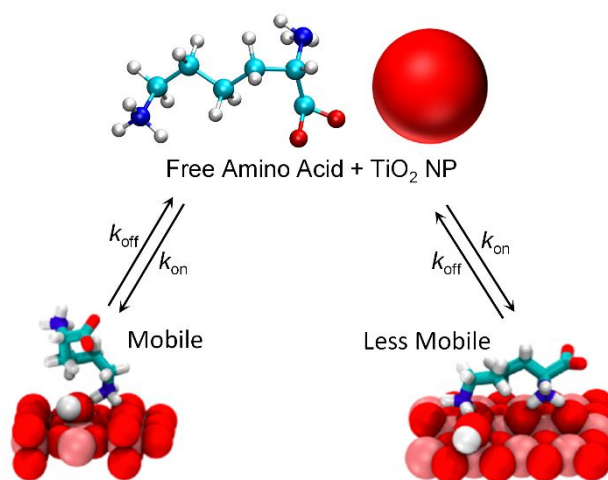


Figure 4. Fitted ^1H DEST profiles for H_δ of 10 mM Arg in the presence of gel and 1 wt % TiO_2 at 50 Hz (a), 150 Hz (b), and 300 Hz (c). Z-spectrums were fitted as the sum of multiple Lorentzian functions. The black dots show the raw data, the red (–) line is the fit of the raw Z function, the dark blue (–) line is the fitted H_δ of arginine centered at 3.16 ppm, the green (–) line is the fitted MT signal or the strongly bound, immobilized species, the purple (–) line is the NOE centered at 1.68 ppm, and the cyan (–) line is the NOE centered at 4.73 ppm. Further discussion of the fitting can be found in the text.

In contrast to Lys and Arg, the DEST profiles for the side chain protons of Asp, Leu and Ala lack the broad component feature (Figures 2c-2d) and NOE intensities to proximal protons are not observed or are much weaker than is the case for protons in Arg and Lys (Figures S3-S5). These data indicate that Asp, Leu, and Ala do not have multiple forms of surface attached species, these amino acids do not display a strongly surface-attached, immobilized form, and reorientational motions are much faster than is the case for Lys and Arg, indicating much weaker interactions with the TiO_2 NP surface.

To obtain surface adsorption/desorption rates, transverse relaxation R_2 rates and the populations of the bulk solution versus adsorbed species, DEST saturation profiles were simulated by numerical solution of the Bloch-McConnell equations.⁴⁹ The multi-Lorentzian fittings to the inverted DEST saturation profiles for 10mM Arg in the presence of TiO_2 NP's indicate presence of at least two adsorbed forms of Arg. The simplest kinetic scheme consistent with the simulated

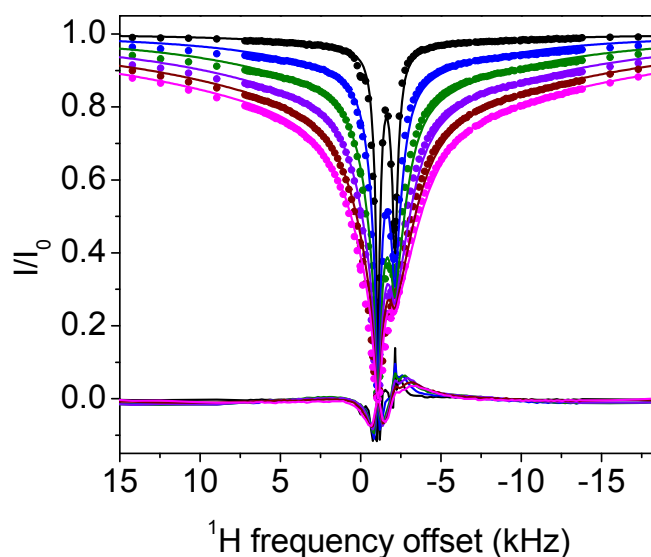
1
2
3 profiles in Figure 4 is shown in Figure 5. Figure 5 is based on a model where monomeric Arg in
4 bulk solution is in exchange with two physically distinct adsorbed forms: a partially mobile bound
5 form and an immobilized bound form. Adsorption of the amino acid in bulk solution to these bound
6 form and an immobilized bound form. Adsorption of the amino acid in bulk solution to these bound
7 forms is characterized by the kinetic constant k_{on} . Desorption from the surface to bulk solution is
8 characterized by k_{off} , respectively. Exchange between the surface-bound forms was excluded from
9 this model.
10
11
12
13
14
15
16
17
18
19
20
21
22
23
24
25
26
27
28
29
30
31
32
33
34
35



36 **Figure 5.** Kinetic Scheme for adsorption of free amino acid onto TiO₂ NP's. The amino acid in
37 bulk solution adsorbs onto the TiO₂ surface in two forms: a partially mobile form and a form that
38 is strongly held on the surface and is more extensively immobilized.
39
40
41

42 ¹H DEST profiles of 10mM Arg in 1 wt % TiO₂ and 1 wt % agarose at a proton Larmor
43 frequency of 700 MHz were simulated using the program DESTfit, according to protocols
44 described in detail in reference 28 and 50. As expected from the multi- Lorentzian fits in
45 Figure 4, the DEST profile for 10mM Arg is fitted best by a model involving exchange
46
47
48
49
50
51
52
53
54
55
56
57
58
59
60

1
2
3 between the amino acid in bulk solution A and two adsorbed forms B and C. The best fit
4
5
6
7 model is shown in Figure 6 and Figure S7, and corresponds to the pseudo-two site
8
9
10 exchange described in reference 28 and 50, where A exchanges with a single kinetic off
11
12
13 rate k_{off} , between a mixture of B and C forms. Notably a two-site exchange model where
14
15
16 A exchanges with a single bound form did not fit the data well. This case is included as
17
18
19
20
21 Supplementary Information (Figure S8). A similar analysis of the ^1H DEST profile for Lys
22
23
24 adsorbed onto TiO_2 NPs is also included in Supplementary Information (Figure S9).
25
26
27



28
29
30
31
32
33
34
35
36
37
38
39
40
41
42
43
44
45
46
47 **Figure 6.** ^1H DEST profiles for H_δ of 10 mM Arg in presence of 1 wt % TiO_2 and 1 wt %
48 agarose on a 700 MHz spectrometer with different B1 saturation fields 50 Hz, 100 Hz,
49 150 Hz, 200 Hz, 250 Hz, and 300 Hz, and global fitting with a homogenous form of
50 McConnell equations using Matlab code DESTfit,^{28,50} where a single spin in exchange
51 between an observable free state A with low R_2 and two bound states (B and C) with
52 larger R_2 values ($A \rightleftharpoons$ the mixture of B and C). The cross-relaxation rate σ_A between
53
54
55
56
57
58
59
60

1
2
3
4 H_δ (the observed signal) and H_γ (coupled with H_δ by cross relaxation) in free Arginine is
5 assumed to be -0.5 s^{-1} , and cross-relaxation rate σ_B between H_δ and H_γ of Arginine bound
6 on particle is assumed to be -500 s^{-1} , the output of global fitting: R_2 (strong binding) =
7 $38785 \pm 119 \text{ s}^{-1}$, R_2 (weak binding) = $784 \pm 2 \text{ s}^{-1}$ with population weights of 0.296 and 0.704,
8 respectively, $k_{\text{off}} = 36.9 \pm 0.1 \text{ s}^{-1}$, $k_{\text{on}} = 2.9 \pm 0.0 \text{ s}^{-1}$, total population of binding state = 0.073,
9 population of free state = 0.927, population of strong binding state = 0.022, population of
10 weak binding state = 0.051.
11
12
13
14
15
16
17

18 **Molecular Dynamics Simulations**

19
20
21 To investigate the nature and origins of structural diversity of adsorbed amino acids at
22 liquid-TiO₂ NP interfaces, and the role played by surface-adsorbed water and surface hydroxyl
23 groups in molecular adsorption, metadynamics was used to compute the binding free energy as a
24 function of amino acid center of mass distance from the non-hydroxylated (Figure 7a) and
25 hydroxylated (Figure 8a) surfaces for Arg and Lys, both of which show broadened DEST profiles
26 in the presence of TiO₂ NP's, as well as Asp, which does not show a broadened DEST profile in
27 the presence of TiO₂ NP's. Calculation of binding free energy is described in the Supporting
28 Information. On both surfaces, we see that Arg is the strongest binder, followed by Lys, and finally
29 Asp. On the non-hydroxylated surface (Figure 7a), there are two free energy minima for Lys and
30 Arg, whereas Asp only shows a single minimum. Interestingly, on the hydroxylated surfaces,
31 although the binding free energies for Arg and Lys are comparable to the non-hydroxylated
32 surface, there is only a single minimum in the binding free energy profile. Asp binds with a lower
33 free energy on the hydroxylated surface compared to the non-hydroxylated surface. The binding
34 free energies for Arg, Lys, and Asp on the non-hydroxylated and hydroxylated surfaces are given
35 in Table 1.
36
37
38
39
40
41
42
43
44
45
46
47
48
49
50
51
52
53
54
55
56
57
58
59
60

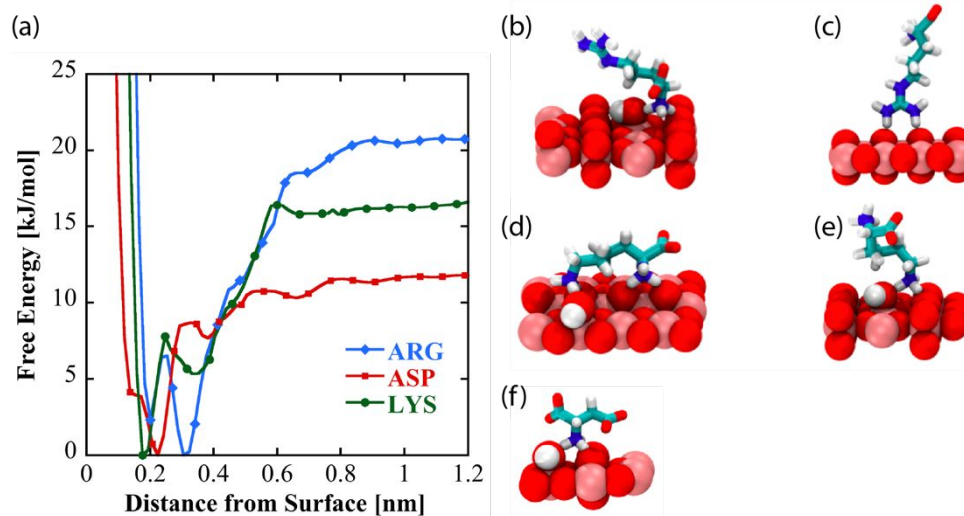


Figure 7: (a) Free energy profiles as a function of amino acid distance from the low-hydroxylated surface of TiO_2 . Dominant binding conformations represented by these curves are shown for arginine (b and c), lysine (d and e), and aspartic acid (f) on the low-hydroxylated surface.

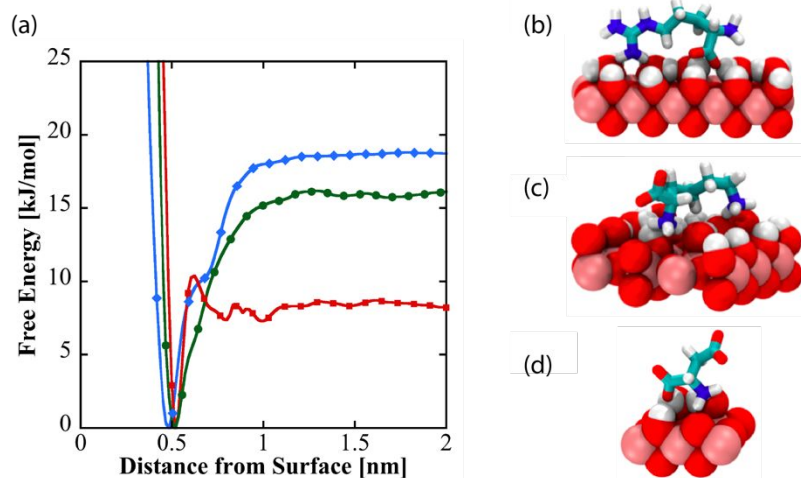


Figure 8: (a) Free energy as a function of amino acid distance from the hydroxylated surface of TiO_2 . Dominant binding conformations are shown for arginine (b), lysine (c), and aspartate (d) on the hydroxylated surface. Note: The peaks in Asp binding profile after

0.5 nm are within the thermal fluctuation (2.5 kJ/mol) at 300K, and does not indicate a different binding mode

	Binding Free Energy (kJ/mol) Non-Hydroxylated Surface		Binding Free Energy (kJ/mol) Hydroxylated Surface
	Mode 1 (flat)	Mode 2 (extended)	
Arginine	-17	-20	-17
Lysine	-15	-10	-15
Aspartate	-10	–	-6

Table 1: Binding free energies for the three amino acids on the two surfaces, in kJ/mol. The binding modes indicate binding poses (flat vs. extended) on the surface.

To understand the structural diversity of the amino acids on the surface, bound structures corresponding to the minima in the free energies for Arg (Figures 7 b-c, Figure 8b), Lys (Figures 7 d-e, Figure 8c), and Asp (Figure 7f, Figure 8d) are shown. On the non-hydroxylated surface, Arg and Lys adopt distinct flat (Figures 7b and 7d, respectively) and extended (Figures 7c and 7e, respectively) conformations. The flat conformation for both (Figures 7b and 7d) is mediated by the binding of the N-terminus, whereas the extended conformation occurs through the sidechain binding. On the hydroxylated surface, both amino acids adopt a flat conformation, mediated by the sidechain and C-terminus. This is in overall agreement with the features of the free energy curve in Figure 8. In contrast, Asp adopts a single conformation on both hydroxylated and non-hydroxylated surfaces. There is also good agreement with prior simulation studies, which report that binding occurs through backbone and side chain associations,⁵⁴ as well as the fact that arginine binding is the strongest.^{32,33}

The binding of amino acids with TiO₂

1
2
3 Study of the binding of amino acids to inorganic oxide NP surfaces, and TiO₂ NP surfaces
4
5 in particular, is motivated by the fact that amino acids serve as models for the binding of more
6
7 complicated polypeptides which are believed to interact with TiO₂ surface hydroxyl groups via
8
9 amino acid side chains. Numerous experimental studies, cited above, have characterized the
10
11 binding affinity of amino acids to TiO₂ NP surfaces. The present DEST NMR study, accompanied
12
13 by a theoretical analysis of binding structures, not only characterizes the binding affinity of five
14
15 amino acids (Arg, Lys, Leu, Asp, Ala) to TiO₂ NP surfaces, but also the kinetics of binding. This
16
17 is accomplished by simulation of the ¹H DEST saturation profiles through solution of the Bloch-
18
19 McConnell equations, which yields R₂ values and populations as well as the kinetic constants that
20
21 quantify exchange between the various free and bound species.
22
23
24
25

26 Kinetic information afforded by DEST simulations are useful both for interpreting the
27
28 relationship between the free and multiple bound states as well as the degree to which interactions
29
30 with the surface immobilizes the various bound molecular forms, where the transverse relaxation
31
32 rate increases with the degree of immobilization of the molecule on the surface. It is interesting to
33
34 compare the results of the DEST study to earlier studies of amino acids bound to TiO₂ surfaces,
35
36 and how kinetic information enhances our view of the binding mechanism. The ¹H DEST NMR
37
38 studies indicate that the amino acids Leu, Ala, and Asp have only a single partly mobile bound
39
40 form in exchange with the freely tumbling amino acid in bulk solution. The Asp result is in accord
41
42 with an earlier Reflectance IR study which detected at least two bound forms of glutamic acid
43
44 (Glu) on TiO₂ surfaces, but a single bound form for Asp.²⁶ The fact that Asp is weakly adsorbed
45
46 onto the TiO₂ NP surface is indicated by its narrow DEST profile which indicates the occurrence
47
48 of reorientational motion even in the bound form. This weak binding is also in accord with the fact
49
50 that at pD 7 the net charge on Asp is negative and TiO₂ has a negative surface charge.
51
52
53
54
55
56
57
58
59
60

1
2
3 From ^1H DEST profiles of side chain protons however, both Arg and Lys have at least two
4 bound forms on TiO_2 NP surfaces, which display in both cases varying degrees of re-orientational
5 motion as indicated by very different R_2 values. An interesting conclusion of the DEST study of
6 Arg involves the relationship between these weakly and strongly bound forms. In the DEST study
7 of cholic acid and phenol to cerium oxide particles by Egner et al.³¹ analysis of DEST saturation
8 profiles for cholic acid indicated only a single weakly bound form. However similar DEST studies
9 of phenol indicated two bound forms: a weakly bound form displaying residual re-orientational
10 motion, and a strongly bound form with a larger R_2 relaxation rate indicating a greater degree of
11 surface immobilization, a similar conclusion to that drawn by our DEST studies of Lys and Arg
12 on TiO_2 NP surfaces. However, the kinetic information derived from the Egner et al study affords
13 a different view of the binding mechanism than is given by the present study of amino acid binding
14 to TiO_2 NP's. With reference to the kinetic scheme in Figure 5, Egner et al. found a best fit to their
15 DEST profile assuming phenol does not directly attach from the bulk solution, where it freely
16 reorients, to the surface, where it is in an immobilized state. Egner et al. also found a finite rate of
17 exchange between the weakly and strongly bound forms, indicating that phenol binds strongly to
18 cerium oxide NP's via a weakly bound intermediate, which retains some reorientational degrees
19 of freedom.
20
21
22
23
24
25
26
27
28
29
30
31
32
33
34
35
36
37
38
39
40
41

42 The DEST analysis of amino acid attachment to TiO_2 NPs presented in this paper indicates
43 a different mechanism of binding between basic amino acids Lys and Arg and rutile TiO_2 NPs than
44 occurs between phenol and cerium oxide NPs. Again with reference to Figure 5, a model that best
45 fits DEST profiles assumes for both Lys and Arg the absence of exchange between the weakly and
46 strongly bound species, and that Lys and Arg in solution interact directly with NP surfaces to form
47 populations of weakly and strongly bound forms.
48
49
50
51
52
53
54
55
56
57
58
59
60

1
2
3 Because exchange between the two bound forms of Lys/Arg is absent in the best fit model
4 to the DEST data, we cannot propose that the partially mobile forms of Lys or Arg are binding
5 intermediates. So we turn to the surface chemistry of TiO₂ as a possible source of variation in
6 binding. It has long been known that dissociative adsorption of water onto rutile surfaces results
7 in the formation of surface hydroxyl groups.^{51,52} Dissociative adsorption of water and subsequent
8 formation of surface hydroxyl groups is known to be face sensitive.⁵³ The surface chemistry
9 observed for TiO₂ NPs is also known to vary with crystal face and surface area.⁵⁴ Therefore, the
10 occurrence of bound Lys and Arg amino acids with different R₂ values may arise when amino
11 acids attach to NP faces with different surface hydroxyl densities, resulting in different degrees of
12 immobilization.
13
14
15
16
17
18
19
20
21
22
23
24
25

26 Molecular dynamics simulations were used to assess the degree to which the variation of
27 surface water and surface hydroxyl groups on the TiO₂ NP surface might account for these multiple
28 bound forms of Lys and Arg. MD simulations in this paper treated two extreme cases: complete
29 absence and presence of surface hydroxyl groups. Under these conditions good qualitative
30 agreement was achieved with ¹H DEST data. For example, on non-hydroxylated surfaces, Arg was
31 found to occur in two forms distinguished by two modes of surface attachment: 1) attachment via
32 the guanidinium group and 2) attachment via the amino group. In each case the opposite end of
33 the amino acid was free to undergo restricted reorientational motions. We propose that these two
34 forms would contribute to the so-called partly mobile bound form observed as a relatively narrow
35 component of the DEST profile of the H δ Arg proton. However, on hydroxylated TiO₂ surfaces,
36 Arg is attached via both its side chain and its amino group, essentially immobilizing the molecule
37 or restricting its motions to a much greater degree than is observed on non-hydroxylated surfaces.
38
39
40
41
42
43
44
45
46
47
48
49
50
51
52
53
54 This would account for the broad components observed in the ¹H DEST profiles of Arg and Lys.
55
56
57
58
59
60

1
2
3
4 The binding mode of Arg on TiO₂ predicted by MD calculations can be further
5
6
7 studied and confirmed experimentally by analysis of relaxation data. For example, the
8
9
10 binding mode of phenol on CeO₂ NP's at atomic resolution was studied based on the
11
12
13 analysis of ¹³C R₂ and R₁ of phenol in the bound state.⁵⁵ Assuming the bound molecule
14
15
16 undergoes rapid restricted rotation on the surface, the ¹³C R₂ of phenol bound on CeO₂
17
18
19 NP's shows a dependence on the angle θ between the C-H bond vector and the axis of
20
21
22 rotation, with maxima in R₂ occurring when the bond vector is parallel ($\theta = 0^\circ$) or
23
24
25 antiparallel ($\theta = 180^\circ$) with the axis of rotation and minimum at angles $\theta = 54.74^\circ$ and
26
27
28 125.26° . In contrast, the ¹³C R₂ of phenol bound with Pt/CeO₂ is independent of the angle
29
30
31 between the C-H bond vector and the axis of rotation, and indicates that the phenol
32
33
34 molecule is rigidly associated with Pt/CeO₂ particle. It will be interesting to similarly
35
36
37 observe the position-specific relaxation of ¹³C-¹H vectors in Arg bound on TiO₂ by solution
38
39
40
41
42
43
44
45 ¹³C NMR to determine the orientation of Arg on TiO₂ surface at atomic resolution. The
46
47
48 results of such a study would further enhance the synergism between solution NMR and
49
50
51
52
53
54
55
56
57
58
59
60 computational methods.

CONCLUSIONS

This paper describes an application of ^1H DEST NMR techniques and Molecular Dynamics (MD) simulations to the study of the kinetics and thermodynamics of biomolecular adsorption onto rutile TiO_2 surfaces. In this work basic amino acids are observed by ^1H DEST experiments to adsorb onto rutile TiO_2 surfaces in multiple forms distinguished by varying degrees of mobility on the surface. Molecular Dynamics simulations indicate that variation in surface hydroxyl group density may be partly responsible for these observations.

Although this study focused on the adsorption of monomeric amino acids onto TiO_2 NP surfaces, ^1H DEST will be useful in general for studying the effect of surface heterogeneity in the binding of larger peptides and proteins to inorganic oxide surfaces. For example, a widely studied surface-binding peptide is the 12 amino acid peptide aptamer i.e. TBP-1 (RKLDPAGMHTW) developed by Sano and coworkers used peptide phage display methodology which electrostatically interacts with the oxidized surface of Ti ¹⁶⁻¹⁸. The N-terminal heaxapeptide RKLPGA is sufficient for TiO_2 . Even in the case of this relatively small peptide, diverse views have been reported for its interactions with TiO_2 surfaces. Sano and coworkers proposed that the positively charged side chain of R1 binds to acidic ($-\text{O}^-$) hydroxyl sites while the negatively charged side chain of D5 binds to basic ($-\text{OH}_2^+$) hydroxyl sites.¹⁶ This binding model was supported by a subsequent adhesion force analysis using AFM.¹⁸ In contrast an NMR study by Suzuki et.al. of TBP-6 bound to TiO_2 NP's concluded that the peptide interacts with the NP surface via the side chains of R1 and K2, while the C-terminal amino acids do not display interactions with the surface.⁵⁶

Based on the results of this study, it is possible that the results of both of these studies are valid. The structure observed by Suzuki et al. may be a partly mobile form with a small R_2 , while the fully immobilized or dark state form reported by Sano and coworkers possesses a much larger

1
2
3 R₂. This situation, which may result from heterogeneity of the NP surface chemistry, could be
4 identified by a ¹H DEST study. We will report such a study in the near future.
5
6
7
8
9
10
11
12
13
14
15
16
17
18
19
20
21
22
23
24
25
26
27
28
29
30
31
32
33
34
35
36
37
38
39

40 *Supporting Information.*

41
42 Well Tempered Metadynamics. ¹H NMR spectra of 10 mM amino acids Lysine, Leucine,
43
44
45
46 Aspartic acid, and Alanine, in the absence of gel, in the presence of gel, and in the
47
48
49 presence of gel and 1 wt % TiO₂. ¹H DEST profiles for H_ε of 10 mM Lysine, Leucine,
50
51
52
53 Aspartate, and Alanine in the absence of gel, in the presence of gel, and in the
54
55
56
57
58
59
60

1
2
3 presence of gel and 1 wt % TiO₂. Deconvoluted ¹H DEST profiles for H_ε of 10 mM Lys as a
4
5
6 function of B₁ field. Simulations of Lys and Arg ¹H DEST profiles using global fitting with a
7
8 homogenous form of McConnell equations using DESTfit. Fitting parameters for Z-spectra of
9
10 Arg and Lys. Summary of kinetic parameters for the binding of 10 mM Arg and Lys with
11
12 TiO₂ using DESTfit. Simulation setup for the arginine (Arg), lysine (Lys), and aspartate (Asp)
13
14
15
16
17
18 on the four titania surfaces.
19
20

21 *Acknowledgements.*
22
23

24 GPD acknowledges National Institutes of Health Grant R21 A126113, NASA grant
25
26
27
28 NNX17AK86G (Exobiology), and National Science Foundation Grant MCB-1715123. GPD
29
30
31 also acknowledges support from collaboration with the University of Oslo through the
32
33
34
35 Research Council of Norway grant 231530.
36
37
38
39
40
41
42
43
44
45
46
47
48
49
50
51
52
53
54
55
56
57
58
59
60

REFERENCES

- (1) Verket, A.; Tiainen, H.; Haugen, H. J.; Lyngstadaas, S. P.; Nilsen, O.; Reseland, J. E. Enhanced osteoblast differentiation on scaffolds coated with TiO₂ compared to SiO₂ and CaP coatings. *Biointerphases* **2012**, *7*, 36.
- (2) Chen, Q. Z.; Thompson, I. D.; Boccaccini, A. R. 45S5 Bioglass[®]-derived glass–ceramic scaffolds for bone tissue engineering. *Biomaterials* **2006**, *27*, 2414–2425.
- (3) Yuan, H.; de Bruijn, J. D.; Zhang, X.; van Blitterswijk, C. A.; de Groot, K. Bone induction by porous glass ceramic made from bioglass[®] (45S5). *J. Biomed. Mater. Res.* **2001**, *58*, 270–276.
- (4) Forsgren, J.; Svahn, F.; Jarmar, T.; Engqvist, H. Formation and adhesion of biomimetic hydroxyapatite deposited on titanium substrates. *Acta Biomater.* **2007**, *3*, 980–984.
- (5) Uchida, M.; Kim, H.; Kokubo, T.; Fujibayashi, S.; Nakamura, T. Structural dependence of apatite formation on titania gels in a simulated body fluid. *J. Biomed. Mater. Res. Part A* **2003**, *64*, 164–170.
- (6) Tiainen, H.; Wohlfahrt, J. C.; Verket, A.; Lyngstadaas, S. P.; Haugen, H. J. Bone formation in TiO₂ bone scaffolds in extraction sockets of minipigs. *Acta Biomater.* **2012**, *8*, 2384–2391.
- (7) Haugen, H.; Will, J.; Köhler, A.; Hopfner, U.; Aigner, J.; Wintermantel, E. Ceramic TiO₂-foams: Characterisation of a potential scaffold. *J. Eur. Ceram. Soc.* **2004**, *24*, 661–668.
- (8) Tiainen, H.; Lyngstadaas, S. P.; Ellingsen, J. E.; Haugen, H. J. Ultra-porous titanium oxide scaffold with high compressive strength. *J. Mater. Sci. Mater. Med.* **2010**, *21*, 2783–2792.

- 1
2
3
4 (9) Jones, F. H. Teeth and bones: Applications of surface science to dental materials
5 and related biomaterials. *Surf. Sci. Rep.* **2001**, 42, 75–205.
6
7
8 (10) Linsebigler, A. L.; Lu, G.; Yates, J. T. Photocatalysis on TiO₂ surfaces: Principles,
9 mechanisms, and selected results. *Chem. Rev.* **1995**, 95, 735–758.
10
11
12 (11) Varghese, O. K.; Grimes, C. A. Metal oxide nanoarchitectures for environmental
13 sensing. *J. Nanosci. Nanotechnol.* **2003**, 3, 277–293.
14
15
16
17 (12) Wintermantel, E.; Eckert, K.-L.; Huang, N.-P.; Textor, M.; Brunette, D. M. Titanium
18 ceramics for cell-carriers and for medical applications; Springer Berlin Heidelberg,
19 **2001**; pp 649–671.
20
21
22
23 (13) Vallee, A.; Humblot, V.; Pradier, C. Peptide interactions with metal and oxide
24 surfaces. *Acc. Chem. Res.* **2010**, 43, 1297–1306.
25
26
27
28 (14) Buckle, E. L.; Lum, J. S.; Roehrich, A. M.; Stote, R. E.; Vandermoon, B.; Dracinsky,
29 M.; Filocamo, S. F.; Drobny, G. P. Serine–lysine peptides as mediators for the
30 production of titanium dioxide: investigating the effects of primary and secondary
31 structures using solid-state NMR spectroscopy and DFT calculations. *J. Phys.*
32 *Chem. B* **2018**, 122, 4708–4718.
33
34
35
36
37 (15) Buckle, E. L.; Prakash, A.; Bonomi, M.; Sampath, J.; Pfaendtner, J.; Drobny, G. P.
38 Solid-state NMR and MD study of the structure of the statherin mutant SNa15 on
39 mineral surfaces. *J. Am. Chem. Soc.* **2019**, 141, 1998–2011.
40
41
42
43 (16) Sano, K.; Shiba, K. A hexapeptide motif that electrostatically binds to the surface
44 of titanium. *J. Am. Chem. Soc.* **2003**, 125, 14234–14235.
45
46
47
48 (17) Sano, K.; Sasaki, H.; Shiba, K. Specificity and biomineralization activities of Ti-
49 Binding Peptide-1 (TBP-1). *Langmuir* **2005**, 21, 3090–3095.
50
51
52
53
54
55
56
57
58
59
60

- 1
2
3
4 (18) Hayashi, T.; Sano, K.-I.; Shiba, K.; Kumashiro, Y.; Iwahori, K.; Yamashita, I.; Hara,
5 M. Mechanism underlying specificity of proteins targeting inorganic materials.
6 *Nano Lett.* **2006**, *6*, 515–519.
7
8
9
10 (19) Chen, Z.; Shen, Y. R.; Somorjai, G. A. Studies of polymer surfaces by sum
11 frequency generation vibrational spectroscopy. *Annu. Rev. Phys. Chem.* **2002**, *53*,
12 437–465.
13
14
15
16 (20) Weidner, T.; Castner, D. G. SFG analysis of surface bound proteins: A route
17 towards structure determination. *Phys. Chem. Chem. Phys.* **2013**, *15*, 12516–
18 12524.
19
20
21
22 (21) Shaw, W. J. Solid-state NMR studies of proteins immobilized on inorganic
23 surfaces. *Solid State Nucl. Magn. Reson.* **2015**, *70*, 1–14.
24
25
26 (22) Zhang, Y.; Xu, H.; Parsons, A. M.; Casabianca L. B. Examining binding to nanoparticle
27 surfaces using saturation transfer difference (STD)-NMR spectroscopy. *J. Phys. Chem. C*
28 **2017**, *121*, 24678–24686.
29
30
31 (23) Okazaki, S.; Aoki, T.; Koichi, T. The adsorption of basic α -amino acids in an
32 aqueous solution by titanium (IV) oxide. *Bull. Chem. Soc. Jpn.* **1981**, *54*, 1595–
33 1599.
34
35
36
37 (24) Roddick-Lanzilotta, A. D.; Connor, P. A.; McQuillan, A. J. An in situ infrared
38 spectroscopic study of the adsorption of lysine to TiO₂ from an aqueous solution.
39 *Langmuir* **1998**, *14*, 6479–6484.
40
41
42
43 (25) Mudunkotuwa, I. A.; Grassian, V. H. Histidine adsorption on tio₂ nanoparticles: An
44 integrated spectroscopic, thermodynamic, and molecular-based approach toward
45 understanding nano–bio interactions. *Langmuir* **2014**, *30*, 8751–8760.
46
47
48
49 (26) Roddick-Lanzilotta, A. D.; McQuillan, A. J. An in situ infrared spectroscopic study
50 of glutamic acid and of aspartic acid adsorbed on TiO₂: Implications for the
51 biocompatibility of titanium. *J. Colloid Interf. Sci.* **2000**, *227*, 48–54.
52
53
54
55
56
57
58
59
60

- 1
2
3 (27) Shchelokov, A.; Palko, N.; Potemkin, V.; Grishina, M.; Morozov, R.; Korina, E.; Uchaev,
4 D.; Krivtsov, I.; Bol'shakov, O. Adsorption of native amino acids on nanocrystalline TiO₂:
5 Physical chemistry, QSPR, and theoretical modeling. *Langmuir* **2019**, *35*, 538–550.
6
7
8 (28) Fawzi, N. L.; Ying, J.; Torchia, D. A.; Clore, G. M. Kinetics of amyloid β monomer-
9 to-oligomer exchange by NMR relaxation. *J. Am. Chem. Soc.* **2010**, *132*, 9948–
10 9951.
11
12
13
14 (29) Fawzi, N. L.; Ying, J.; Ghirlando, R.; Torchia, D. A.; Clore, G. M. Atomic-resolution
15 dynamics on the surface of amyloid- β protofibrils probed by solution NMR. *Nature*
16 **2011**, *480*, 268–272.
17
18
19
20 (30) Fawzi, N. L.; Libich, D. S.; Ying, J.; Tugarinov, V.; Clore, G. M. Characterizing
21 methyl-bearing side chain contacts and dynamics mediating amyloid β protofibril
22 interactions using ¹³C_{methyl}-DEST and lifetime line broadening. *Angew. Chem. Int.*
23 *Ed.* **2014**, *53*, 10345–10349.
24
25
26
27
28 (31) Egner, T. K.; Naik, P.; Nelson, N. C.; Slowing, I. I.; Venditti, V. Mechanistic insight
29 into nanoparticle surface adsorption by solution NMR spectroscopy in an aqueous
30 gel. *Angew. Chem. Int. Ed.* **2017**, *129*, 9934–9938.
31
32
33
34 (32) Yazdanyar, A.; Aschauer, U.; Bowen, P. Adsorption free energy of single amino acids at
35 the rutile (110)/water interface studied by well-tempered metadynamics. *J. Phys. Chem. C*
36 **2018**, *122*, 11355–11363.
37
38
39 (33) Kang, Y.; Li, X.; Tu, Y.; Wang, Q.; Ågren, H. On the mechanism of protein adsorption
40 onto hydroxylated and nonhydroxylated TiO₂ surfaces. *J. Phys. Chem. C* **2010**, *114*,
41 14496–14502.
42
43
44 (34) Brandt, E. G.; Lyubartsev, A. P. Molecular dynamics simulations of adsorption of amino
45 acid side chain analogues and a titanium binding peptide on the TiO₂ (100) surface. *J.*
46 *Phys. Chem. C* **2015**, *119*, 18126–18139.
47
48
49 (35) Skelton, A. A.; Liang, T.; Walsh, T. R. Interplay of sequence, conformation, and binding
50 at the peptide–titania interface as mediated by water. *ACS Appl. Mater. Interfaces* **2009**,
51 *1*, 1482–1491.
52
53
54 (36) Sultan, A. M.; Hughes, Z. E.; Walsh, T. R. Binding affinities of amino acid analogues at
55 the charged aqueous titania interface: implications for titania-binding peptides. *Langmuir*
56 **2014**, *30*, 13321–13329.
57
58
59
60

- 1
2
3
4 (37) Zhou, I. Y.; Wang, E.; Cheung, J. S.; Zhang, X.; Fulci, G.; Sun, P. Z. Quantitative
5 chemical exchange saturation transfer (CEST) MRI of glioma using Image
6 Downsampling Expedited Adaptive Least-squares (IDEAL) fitting. *Sci. Rep.* **2017**,
7 7, 84.
8
9
10
11 (38) Cai, K.; Singh, A.; Poptani, H.; Li, W.; Yang, S.; Lu, Y.; Hariharan, H.; Zhou, X. J.;
12 Reddy, R. CEST signal at 2ppm (CEST@2ppm) from Z-spectral fitting correlates
13 with creatine distribution in brain tumor. *NMR Biomed.* **2015**, 28, 1–8.
14
15
16
17 (39) Zaiss, M.; Windschuh, J.; Paech, D.; Meissner, J.-E.; Burth, S.; Schmitt, B.;
18 Kickingeder, P.; Wiestler, B.; Wick, W.; Bendszus, M.; Schlemmer, H.-P.; Ladd,
19 M. E.; Bachert, P.; Radbruch, A. Relaxation-compensated CEST-MRI of the
20 human brain at 7 T: Unbiased insight into NOE and amide signal changes in
21 human glioblastoma. *NeuroImage* **2015**, 112, 180–188.
22
23
24
25
26
27 (40) Zhang, X.-Y.; Wang, F.; Afzal, A.; Xu, J.; Gore, J. C.; Gochberg, D. F.; Zu, Z. A
28 new NOE-mediated MT signal at around -1.6 ppm for detecting ischemic stroke
29 in rat brain. *Magn. Reson. Imaging* **2016**, 34, 1100–1106.
30
31
32
33 (41) Zhang, X.; Wang, F.; Jin, T.; Xu, J.; Xie, J.; Gochberg, D. F.; Gore, J. C.; Zu,
34 Z. MR imaging of a novel NOE-mediated magnetization transfer with water in rat
35 brain at 9.4T. *Magn. Reson. Med.* **2017**, 78, 588–597.
36
37
38
39 (42) Předota, M.; Bandura, A. V.; Cummings, P. T.; Kubicki, J. D.; Wesolowski, D. J.;
40 Chialvo, A. A.; Machesky, M. L. Electric double layer at the rutile (110) surface. 1.
41 Structure of surfaces and interfacial water from molecular dynamics by use of ab
42 initio potentials. *J. Phys. Chem. B* **2004**, 108, 12049–12060.
43
44
45
46
47 (43) Huang, J.; MacKerell Jr, A. D. CHARMM36 all-atom additive protein force field :
48 Validation based on comparison to NMR data. *J. Comput. Chem.* **2013**, 34, 2135–
49 2145.
50
51
52
53
54
55
56
57
58
59
60

- 1
2
3
4 (44) Bussi, G.; Donadio, D.; Parrinello, M. Canonical sampling through velocity
5 rescaling. *J. Chem. Phys.* **2007**, 126, 014101.
6
7
8 (45) Parrinello, M.; Rahman, A. Polymorphic transitions in single crystals: A new
9 molecular dynamics method. *J. Appl. Phys.* **1981**, 52, 7182.
10
11
12 (46) Barducci, A.; Bussi, G.; Parrinello, M. Well-tempered metadynamics: A smoothly
13 converging and tunable free-energy method. *Phys. Rev. Lett.* **2008**, 100, 020603.
14
15
16
17 (47) Abraham, M. J.; Murtola, T.; Schulz, R.; Páll, S.; Smith, J. C.; Hess, B.; Lindahl, E.
18 GROMACS: High performance molecular simulations through multi-level
19 parallelism from laptops to supercomputers. *SoftwareX*, **2015**, 1–2, 19–25.
20
21
22
23 (48) Tribello, G. A.; Bonomi, M.; Branduardi, D.; Camilloni, C.; Bussi, G. PLUMED 2:
24 New feathers for an old bird. *Comput. Phys. Commun.* **2014**, 185, 604–613.
25
26
27
28 (49) Helgstrand, M.; Härd, T.; Allard, P. Simulations of NMR pulse sequences during
29 equilibrium and non-equilibrium chemical exchange. *J. Biomol. NMR* **2000**, 18,
30 49–63.
31
32
33
34 (50) Fawzi, N. L.; Ying, J.; Torchia, D. A.; Clore, G. M. Probing exchange kinetics and
35 atomic resolution dynamics in high-molecular-weight complexes using dark-state
36 exchange saturation transfer NMR spectroscopy. *Nat. Protoc.* **2012**, 7, 1523–
37 1533.
38
39
40
41 (51) Connor, P. A.; Dobson, K. D.; McQuillan, A. J. Infrared spectroscopy of the
42 TiO₂/aqueous solution interface. *Langmuir* **1999**, 15, 2402–2408.
43
44
45 (52) Henderson, M. A. The interaction of water with solid surfaces: fundamental aspects
46 revisited. *Surf. Sci. Rep.* **2002**, 46, 1–308.
47
48
49 (53) Henderson, M. A. Structural sensitivity in the dissociation of water on TiO₂ single-crystal
50 surfaces. *Langmuir* **1996**, 12, 5093–5098.
51
52
53 (54) Bolis, V.; Busco, C.; Ciarletta, M.; Distasi, C.; Erriquez, J.; Fenoglio, I.; Livraghi, S.; Morel,
54 S. Hydrophilic/hydrophobic features of TiO₂ nanoparticles as a function of crystal phase,
55
56
57
58
59
60

1
2
3 surface area and coating, in relation to their potential toxicity in peripheral nervous system.
4 *J. Colloid Interface Sci.* **2012**, 369, 28–39.
5

- 6
7 (55) Egner, T. K.; Naik, P.; An, Y.; Venkatesh, A.; Rossini, A. J.; Slowing, I. I.; Venditti, V.
8 ‘Surface Contrast’ NMR reveals non-innocent role of support in Pd/CeO₂ catalyzed phenol
9 hydrogenation. *ChemCatChem* **2020**, DOI: 10.1002/cctc.202000608.
10
11 (56) Suzuki, Y.; Shindo, H.; Asakura, T. Structure and dynamic properties of a Ti-binding
12 peptide bound to TiO₂ nanoparticles as accessed by ¹H NMR spectroscopy. *J. Phys. Chem.*
13 *B* **2016**, 120, 4600–4607.
14
15
16
17
18
19
20
21
22
23
24
25
26
27
28
29
30
31
32
33
34
35
36
37
38
39
40
41
42
43
44
45
46
47
48
49
50
51
52
53
54
55
56
57
58
59
60

For Table of Contents Only:

